

Room-Temperature Quantum Emitter in Aluminum Nitride

Sam G. Bishop, John P. Hadden, Faris D. Alzahrani, Reza Hekmati, Diana L. Huffaker, Wolfgang W. Langbein, and Anthony J. Bennett*

Cite This: <https://dx.doi.org/10.1021/acsp Photonics.0c00528>

Read Online

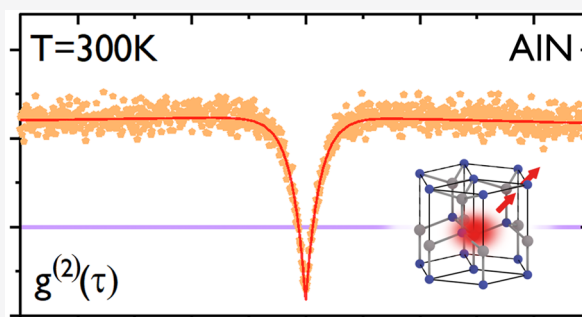
ACCESS |

Metrics & More

Article Recommendations

ABSTRACT: A device that is able to produce single photons is a fundamental building block for a number of quantum technologies. Significant progress has been made in engineering quantum emission in the solid state, for instance, using semiconductor quantum dots as well as defect sites in bulk and two-dimensional materials. Here we report the discovery of a room-temperature quantum emitter embedded deep within the band gap of aluminum nitride. Using spectral, polarization, and photon-counting time-resolved measurements we demonstrate bright ($>10^5$ counts s^{-1}), pure ($g^{(2)}(0) < 0.2$), and polarized room-temperature quantum light emission from color centers in this commercially important semiconductor.

KEYWORDS: aluminum nitride, single photon source, quantum optics, room temperature



Recently, there has been renewed interest in the group III-nitrides as platforms for quantum optics. In the past few years, point-like single photon sources have been reported in hexagonal boron nitride,¹ gallium nitride (GaN),^{2–4} and, very recently, aluminum nitride (AlN).^{5,6} By virtue of their deep confinement energies, these color centers demonstrate antibunching even at room temperature, adding to a select group of solid state materials that host high-temperature quantum emitters, such as diamond^{7–9} and silicon carbide (SiC).^{10–12} The commercial applications of the nitrides means there is considerable expertise in processing and the possibility of epitaxial deposition of complex heterostructures, paving the way to cavity enhancement and optoelectronic devices.

AlN is a semiconductor with a large band gap of 6.2 eV, making it a promising platform for integrated quantum photonic applications^{13–16} due to its transparency in the visible spectrum, strong second-order nonlinearity,¹³ low-loss high-speed opto-electric phase modulation,¹⁴ mature device fabrication, and available high-purity substrates. In its wurtzite phase, AlN has a hexagonal unit cell, shown in Figure 1a, that lacks inversion-symmetry along the [0001] crystallographic axis. This, along with the finite dipole moment associated with the aluminum–nitrogen bond, leads to internal electric polarization and piezoelectric effect along [0001]. Recently, AlN has been predicted to host atomic-like defects with optically addressable spin states,^{17–20} which would be ideal for quantum technologies that require an interface between flying photonic qubits and stationary trapped spin qubits. The emitters we observe here have a narrow distribution in zero-phonon line energy and a prominent phonon sideband. This

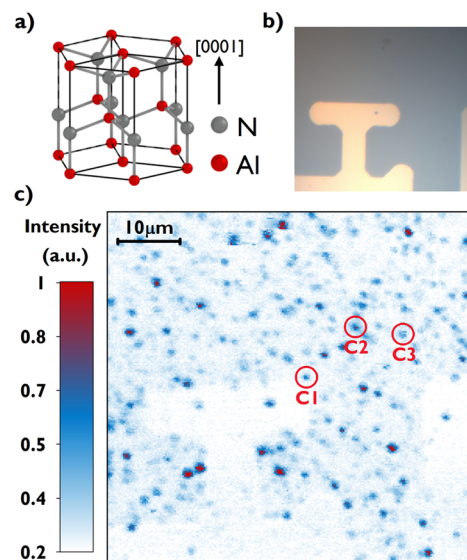


Figure 1. Confocal mapping of point-like emitters in AlN. (a) Crystal structure of aluminum nitride. The polar crystal axis [0001] is indicated. (b) Optical image of the sample with titanium markers. (c) Intensity scan map of the sample. The three emitters, C1–C3, studied in this work are labeled.

Received: April 2, 2020

Published: June 11, 2020

suggests the emitters in our sample all arise from the same crystal defect.⁶

RESULTS AND DISCUSSION

The sample studied within this work is a 1 μm thick epilayer of AlN-on-sapphire. A confocal scanned optical image of the sample shown in Figure 1c reveals the presence of point-like emitters. A titanium mask on the sample surface is visible, which enables identification of an emitters' position. The emitter density is estimated to be $1.25 \mu\text{m}^{-2}$, which is sufficient for individual emitters to be optically addressed with a diffraction limited optical spot.

Three color centers, C1–C3, are labeled on the scan map and subsequently studied in detail in Figure 2. Spectra of the three emitters shown in Figure 2a have an obvious spectral peak labeled as a zero phonon line (ZPL) at 2.08, 2.12, and 2.09 eV, respectively. This is attributed to the optical excited-to-ground state transition of the color centers without high-energy phonon emission, by analogy with the ZPL observed in the NV^- center in diamond, which has a room-temperature ZPL at 1.95 eV.⁷ In addition to the ZPL peak, each emitters' spectrum demonstrates coupling to high-energy phonons apparent as a broad phonon sideband (PSB), spanning about 0.6 eV to the red. Such a broad, prominent, PSB has not been reported in other nitride emitters,^{2,4} but qualitatively resembles that of the NV^- in diamond.⁸

The room-temperature FWHM of the ZPLs are 8.3 ± 0.3 , 11.7 ± 0.2 , and 9.4 ± 0.2 meV, respectively. Broadening of the ZPL at room temperature is consistent with coupling to low energy acoustic phonon modes and spectral jitter. The ZPL contains 3.2% of the total intensity on average. However, enhancement of the light emitted into the ZPL in a phonon-broadened emitter by weak coupling to an optical cavity has been demonstrated in other materials.²¹ The spectra for the emitters C2 and C3 have significantly different PSBs. The cause of the change in spectral shapes may result from emitters located in different strain fields or in proximity to crystal dislocations and impurities.

The quantum nature of the emitters is proven in Figure 2a, which shows the result of Hanbury Brown and Twiss autocorrelation measurements, under 532 nm excitation at 350 μW at room temperature. The emission was filtered between 1.91 and 2.33 eV, to suppress the fluorescence signal from the Cr^{3+} impurity in the sapphire substrate.²² Antibunching below the $g^{(2)}(\tau) < 0.5$ limit is observed. $g^{(2)}(0)$ for the three emitters C1–C3 are 0.17 ± 0.01 , 0.20 ± 0.01 , and 0.23 ± 0.02 , respectively. The phonon energies available within AlN can be determined from a Stokes-shifted Raman measurement, as is shown in Figure 2c. The measurement can provide an insight into Raman-active phonon modes: it is possible to identify a number of vibrational energies from both the AlN and sapphire.^{23,24} The response of the sapphire substrate is to be expected given to the limited axial resolution of the confocal microscope with respect to the AlN thickness. Using the relation $\Delta E = E_{\text{ZPL}} - E_{\text{PX}}$, where E_{PX} is the peak energy for P1–P5 in the spectrum for emitter C1, it is possible to correlate the Raman shift due to the vibrational modes from the AlN with the peak locations. Ignoring the contributions due to vibrational modes from the sapphire, the Raman-shifted transitions ΔE ; E_2^{LOW} , Al^{TO} , E_2^{HIGH} and Al^{LO} are given as 31.2 ± 0.1 , 76.7 ± 0.3 , 81.70 ± 0.01 , and 110.3 ± 0.1 meV, respectively. Therefore, we hypothesize that the peaks P1 and P3 arise due to phonon

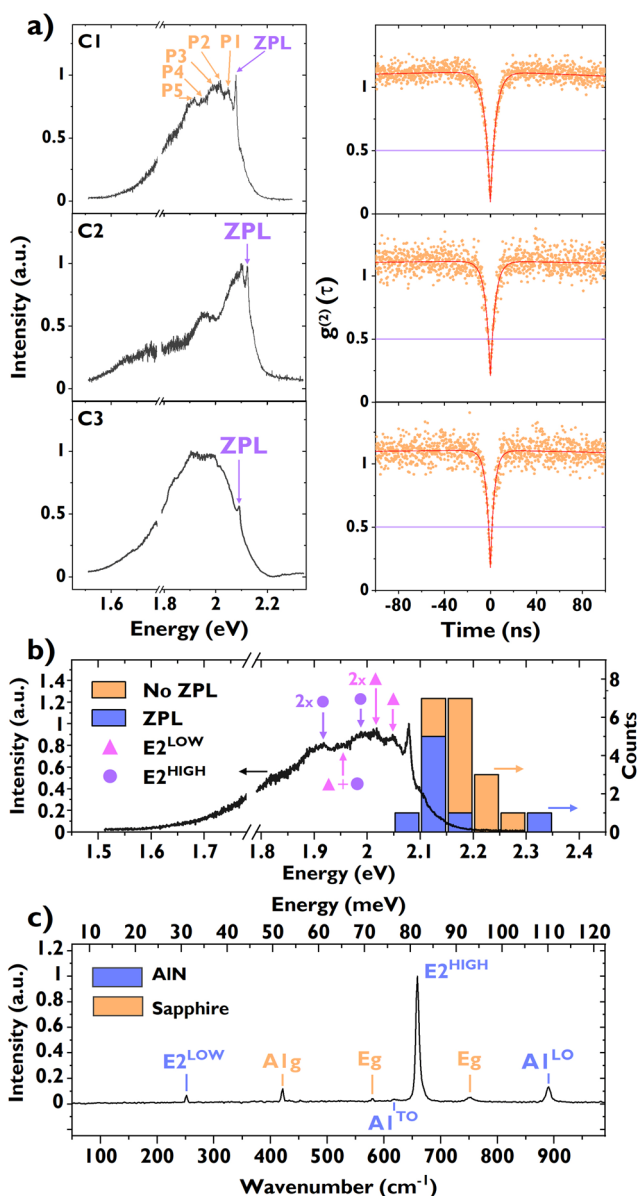


Figure 2. Room-temperature spectroscopy of color centers in AlN. (a) Spectral and autocorrelation measurements of the three emitters, labeled C1, C2, and C3 in the intensity scan map in Figure 1c. (b) Histogram showing the energy in which the spectra for 20 emitters has fallen to half its maximum intensity, on the high energy side. The orange data represents emitters where an obvious zero phonon line cannot be identified. The spectrum for C1 is overlaid, with phonon-shifted energies of the zero phonon line labeled. (c) Raman spectrum showing phonon modes in the AlN on sapphire substrate.

assisted replicas from coupling to E_2^{LOW} and E_2^{HIGH} , respectively, as well as peaks P2 and P5 from the corresponding two-phonon processes. In addition, P4 may be described by a mixed two phonon emission involving $E_2^{\text{LOW}} + E_2^{\text{HIGH}}$. These phonon-replica peaks are illustrated in Figure 2b. We hypothesize the higher energy peaks arise from interactions with multiple-phonon-assisted transitions and the broadening from the small defect size coupling to a large range of the phonon density of states²³ in the Brillouin zone. Comparable peaks are not as pronounced in the spectra from C2 and C3, due to the contributions merging into a single PSB. Comparatively, the reduced dimensionality of the h-BN system

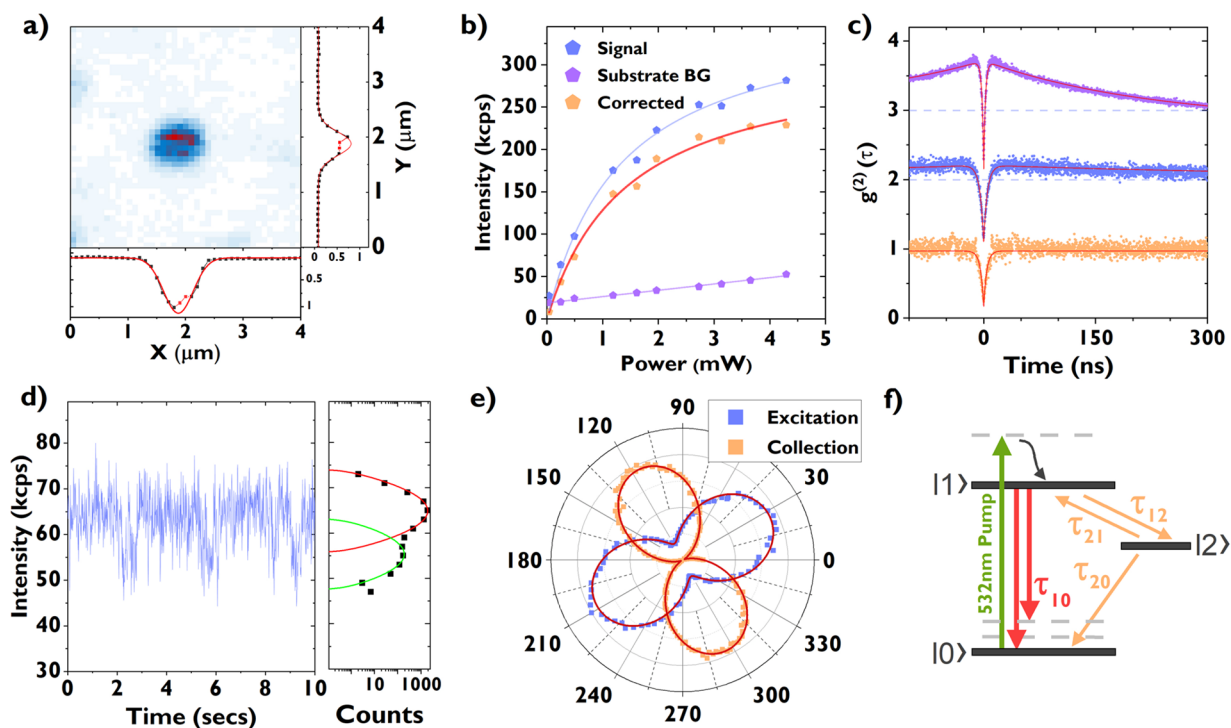


Figure 3. Photostability, autocorrelation, polarization, and power dependence of C1 at room temperature. (a) Confocal scan over the emitter, with an accompanying X and Y slice. (b) Power-dependent measurement of intensity showing saturation of intensity at high pump laser power. (c) Autocorrelation measurement at a pump power of 30 μ W (orange), 350 μ W (blue), and 3.2 mW (purple), demonstrating both room-temperature antibunching and bunching. (d) Time-resolved stability measurement. (e) Polarization measurement in both excitation and collection. (f) Illustration of the three energy level model used to fit the data in (c).

results in a strikingly different phonon-spectrum consisting of replicas of the ZPL spaced by optical photon frequencies with the fraction of the total emission via the ZPL as high as 0.82.¹ Conversely previous reports on color centers in GaN^{2,4} and AlN⁵ do not report high-energy phonon sidebands, where the emitters reported here bear a closer resemblance to the NV center in diamond.⁸

A histogram illustrating the energies of 20 emitters, with a bin width of 50 meV, is shown in Figure 2b. All emitters showed a broad emission shape with a ZPL not always being resolved. Therefore, a half max (HM) value is defined that corresponds to the energy at which each spectrum, at the higher energy side, has fallen to half its highest intensity. The same HM value was defined for spectra that have an obvious ZPL (purple) as well as for no obvious ZPL (orange). The histogram illustrates that the majority of the emitters have their HM between 2.10 and 2.25 eV, corresponding to ZPLs between 2.00 and 2.15 eV. This represents a smaller spectral distribution as compared to color centers recently discovered in GaN, where the ZPL energy between emitters within the same sample varies over 0.4 eV.² The smaller variation in the ZPL energy for these AlN emitters provides obvious advantage for their exploitation in photonic and/or optoelectronic devices coupled to narrowband cavities or antennae. In addition, it suggests a common origin for all the emitters we have observed in AlN, with energy shifts between emitters resulting from differences in strain, local dislocation density, impurities, or point defects.

The scan image in Figure 1c shows that some defects are unstable on a time scale comparable to the 10 ms dwell time of each pixel. This is also apparent in the confocal scan around the color center C1 shown in Figure 3a. Intensity slices in both

the X and Y axis are presented which demonstrate the diffraction limited size of the emission from the color center C1. The excitation power (P) dependence of the emission intensity of C1 is shown in Figure 3b. The data were fitted with the relation $I(P) = I_{\infty} \times P / (P + P_{\text{sat}})$. The saturation intensity $I(P_{\text{sat}}) = 157$ kcps at $P_{\text{sat}} = 1.44$ mW, which demonstrates the brightness of the emitters at room temperature. The emitter brightness, $>10^5$ counts s^{-1} at high saturation power, is consistent with other III-nitride emitters in a high-refractive index bulk.^{2,5}

Intensity autocorrelation measurements as a function of excitation power are presented in Figure 3c, vertically offset for clarity. Antibunching on a 4.1 ± 0.2 ns time scale is observed in parallel with bunching on a 208.5 ± 0.7 ns nanosecond time scale at the highest pump power. The amplitude of the bunching is greater at increasing excitation power, indicative of an internal energy structure that is more complex than a two-level emitter. We use rate equations⁸ to obtain a good fit, by including a metastable state, which "shelves" the excitation for a finite time greater than the recombination rate of the excited-to-ground state transition. An illustration of the energy level system is shown in Figure 3f, the shelving rate being given by τ_{12} . The purity of the emission is given by $g^{(2)}(0) = 0.19 \pm 0.01$ at $P = 30$ μ W. Photon bunching at room temperature is also observed in diamond NV centers,⁸ SiC,¹² h-BN,¹ and GaN color centers,²⁻⁵ with antibunching time scales having the same order of magnitude.

A stability measurement, where the number of photons incident on an avalanche photodiode is recorded every 10 ms for a total of 60 s, is presented in Figure 3d. The plot shows a 10 s snapshot of the intensity detected, showing intermittent variations between two fluorescence intensities, one centered

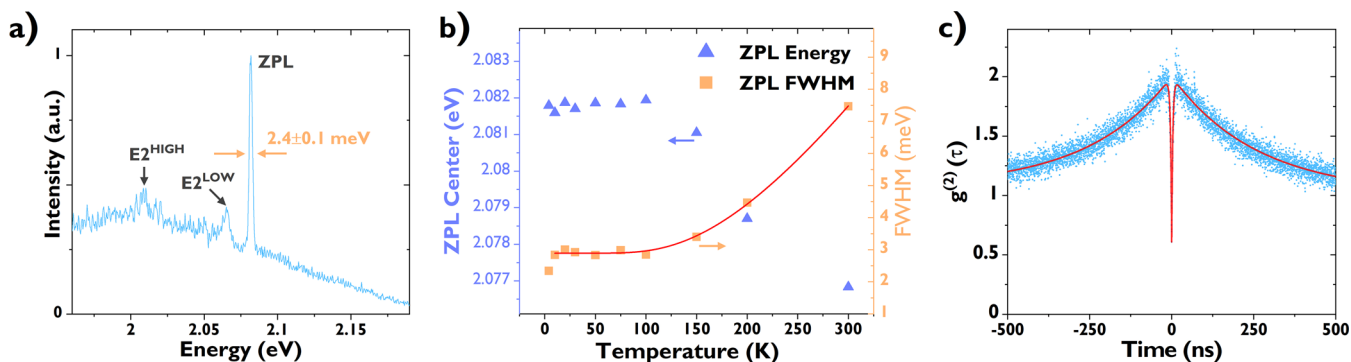


Figure 4. Temperature dependence, spectral, and autocorrelation measurements of C1 at low temperature. (a) Photoluminescence spectrum of C1 at 4 K. (b) Temperature dependence of the zero phonon line energy and full width half-maximum between 4 and 300 K. (c) Autocorrelation measurement at 4 K under 532 nm excitation at 4 mW.

at 63 kcps and the other at 55 kcps. A statistical analysis of the intensities seen over the whole 60 s measurement is presented, whereby the intensities are binned into 2 kcps bins. The data is fit with two Gaussian distributions with the same width, where the $\text{HWHM} \times e^{-1/2}$ variance represents the shot noise of \sqrt{n} associated with detecting n photons per sampling event. For the more frequently occurring fluorescent state, an average of 630 counts per 10 ms are detected, giving a noise value of 2.5 kcps in the presented measurement. The occurrence of the less intense fluorescence state is 9%. This instability is observed in a number of other emitters, but not all, and is reported for other III-nitride color centers. We hypothesize that this instability is not caused by shelving the carrier into the metastable state, as the switching has a time scale orders of magnitude greater than the bunching observed in the $g^{(2)}(t)$ measurement in Figure 3c, but rather is caused by an additional noise source such as a nearby impurity periodically charging and discharging.

A measurement of the emission intensity from C1 as the linear polarization of the excitation or collection beam are rotated in the plane of the sample is presented in Figure 3e. For the collection measurement, the excitation polarization is aligned to its maximum. Both excitation and collection data demonstrate dipole-like emission patterns. The ratio in intensity between the maximum and minimum is 5:1 and 70:1 in the absorption and emission, respectively. This linear polarization is observed for all emitters suggesting their excitonic dipole is always orientated in the plane of the sample. An angular difference between the maxima in absorption and emission polarizations is consistent with other reports on III-nitride color centers.^{2,3,5} We hypothesize that this is due to a multilevel energy structure with excitation and emission transitions having orthogonal polarization selection rules in the plane of the sample. The absorption and emission dipoles for C1 and C3 are orientated parallel to the $[\bar{1}2\bar{1}0]$ plane and m -plane $[10\bar{1}0]$, respectively. In addition, polarization measurements for C2 demonstrate linearly polarized collection 35° offset to the m -plane, along the $[11\bar{2}0]$ plane.

To gain insight into the temperature dependent properties of the emitters the sample was cooled to 4 K using a closed-cycle helium cryostat. A spectrum of emitter C1 at 4 K is presented in Figure 4a. A sharpening of the ZPL is observed, as coupling with phonon modes is reduced at lower temperature. The intensity of the emission decreases by a factor of 2 on reducing the temperature from 300 to 4 K.

The ZPL FWHM at 4 K is 2.4 ± 0.1 meV, which is an order of magnitude above the resolution limit of the spectrometer. The temperature dependence of the FWHM (orange) and the zero phonon line energy E_{ZPL} (purple) is presented in Figure 4b. The FWHM follows a Bose-activated broadening from 10 to 300 K, described by $\gamma = \gamma_0 + \beta/(e^{E/k_B T} - 1)$, where γ_0 is a temperature-independent broadening, E is the activation energy, and β is the coupling coefficient. A good fit to the data is achieved with the parameters; $\gamma_0 = 2.90 \pm 0.04$ meV, $\beta = 29.7 \pm 0.4$ meV, and $E = 52.0 \pm 0.3$ meV. The second-order correlation measurement in Figure 4c, taken at 4.0 mW excitation power, confirms the photon statistics at low temperature are comparable to the behavior measured under ambient conditions (Figure 3c).

CONCLUSION

Quantum emission from the sample is attributed to point-like defects embedded deep within the band gap of AlN. The below band gap excitation used here suggests that the defect states are directly being excited. The nature of the emitters is unknown, but several theoretical studies have predicted and studied spin-dependent defects in AlN.^{17–20} Secondary ion mass spectrometry (SIMS) measurements from the manufacturer (Dowa Electronics Materials Co.) show trace levels of hydrogen, carbon, oxygen, and silicon in the sample. In the future, controlled introduction of other impurities via direct growth or implantation may enable us to engineer desirable spin systems in AlN. Control of the spin states may be possible via the piezoelectric effect, similar to what has been achieved in emitters in SiC¹⁰ or through resonant optical fields. The cross-polarized maxima in emission and absorption dipoles presents an ideal arrangement for efficient polarization filtered resonant control, which conventionally limits the efficiency to 50% due to the perpendicular excitation and detection optics required to isolate the laser.²⁵ Owing to significant existing investment in AlN transducers and sensors this material may be able to compete with diamond and SiC as a viable platform for quantum technologies if it can be shown to host spin-dependent emission from the color centers: in these other materials optical manipulation and read-out of color center spin states^{9,26} has enabled sensitive nanoscale sensing^{27,28} and promising room-temperature qubits.

METHODS

Room-temperature measurements were taken on a confocal microscope with a 0.9 NA microscope objective. The

collection efficiency is calculated to be 5.1% into the first lens,²⁹ assuming a dipole orientated in the plane and with a refractive index $n_{\text{AlN}} = 2.15$ at 600 nm. Low-temperature and temperature-dependent measurements were taken in an AttoDry 1000 closed-cycle helium cryostat with an internal 0.68 NA aspheric lens and a custom optical head. The collection efficiency into the first lens is 2.5%. Single mode fiber is used to couple both the excitation and the collection into/out of both the room-temperature and cryostat microscopes.

Room-temperature confocal images were obtained by scanning the laser using dual-axis galvanometric mirrors within a optical 4F system. Excitation and collection polarization measurements was measured using a linear polarizer followed by a half-wave plate in the excitation path and a thin film polarizer in the collection path.

Time-resolved measurements were taken using two SPCM-AQRH silicon avalanche photodiodes, with unbalanced dark count rates of 50 and 520 cps, respectively. Autocorrelation measurements were taken using a 45:55 fiber beamsplitter. The y -axis offset at time zero in the autocorrelation measurements can be accounted for by including unbalanced dark-count rates, B_1 and B_2 , on the two detectors, shown in eq 1. S_1 and S_2 are the signal count rates on the detectors, 4700 and 3650 cps, respectively, and $C_N(\tau)$ the normalized coincidence amplitude at large delay times. After correction, for C1 under 30 μW excitation, we find $g^{(2)}(0) = 0.06$.

$$g^{(2)}(\tau) = C_N(\tau) \frac{S_1 S_2 + 2S_1 B_2 + 2S_2 B_1 + B_1 B_2}{S_1 S_2} - \frac{2S_1 B_2 + 2S_2 B_1 + B_1 B_2}{S_1 S_2} \quad (1)$$

A frequency doubled continuous-wave 532 nm Nd:Yag laser was used for excitation in all measurements. Optical filtering was achieved using a ultrastep 532 nm long-pass filter to enable Raman spectroscopy and a short pass 650 nm filter to isolate the color center emission from the Cr^{3+} emission (1.78 eV) from the sapphire.² For spectral measurements beyond 650 nm as presented in Figure 2a, the 650 nm short pass filter is removed and we background correct using a spectrum taken from an area close to the emitter, which represents emission from the substrate. In the future, the study of free-standing AlN or AlN-on-silicon samples would eliminate the need for this spectral filtering.

AUTHOR INFORMATION

Corresponding Author

Anthony J. Bennett – School of Engineering, Cardiff University, Cardiff CF24 3AA, United Kingdom; Email: bennetta19@cardiff.ac.uk

Authors

Sam G. Bishop – School of Engineering, Cardiff University, Cardiff CF24 3AA, United Kingdom; orcid.org/0000-0001-6353-6601

John P. Hadden – School of Physics and Astronomy, Cardiff University, Cardiff CF24 3AA, United Kingdom; orcid.org/0000-0001-5407-6754

Faris D. Alzahrani – School of Physics and Astronomy, Cardiff University, Cardiff CF24 3AA, United Kingdom

Reza Hekmati – School of Physics and Astronomy, Cardiff University, Cardiff CF24 3AA, United Kingdom

Diana L. Huffaker – School of Engineering and School of Physics and Astronomy, Cardiff University, Cardiff CF24 3AA, United Kingdom

Wolfgang W. Langbein – School of Physics and Astronomy, Cardiff University, Cardiff CF24 3AA, United Kingdom

Complete contact information is available at:

<https://pubs.acs.org/10.1021/acsp Photonics.0c00528>

Notes

The authors declare no competing financial interest.

The data that supports this publication are at <http://doi.org/10.17035/d.2020.0110094158>.

ACKNOWLEDGMENTS

The authors thank the financial support provided by the Sêr Cymru National Research Network in Advanced Engineering and Materials, the European Union's Horizon 2020 research and innovation program and the Royal Society for Research Grant RGS191251, and EPSRC Grant EP/T017813/1. Since submission of this manuscript, the authors were made aware of a report of single photon emission from defects in AlN by Xue et al.⁵

REFERENCES

- (1) Tran, T. T.; Bray, K.; Ford, M. J.; Toth, M.; Aharonovich, I. Quantum emission from hexagonal boron nitride monolayers. *Nat. Nanotechnol.* **2016**, *11*, 37–41.
- (2) Berhane, A. M.; Jeong, K.-Y.; Bodrog, Z.; Fiedler, S.; Schröder, T.; Triviño, N. V.; Palacios, T.; Gali, A.; Toth, M.; Englund, D.; Aharonovich, I. Bright Room-Temperature Single-Photon Emission from Defects in Gallium Nitride. *Adv. Mater.* **2017**, *29*, 1605092.
- (3) Zhou, Y.; Wang, Z.; Rasmita, A.; Kim, S.; Berhane, A.; Bodrog, Z.; Adamo, G.; Gali, A.; Aharonovich, I.; Gao, W.-b. Room temperature solid-state quantum emitters in the telecom range. *Science Advances* **2018**, *4*, No. ear3580.
- (4) Nguyen, M.; Zhu, T.; Kianinia, M.; Massabuau, F.; Aharonovich, I.; Toth, M.; Oliver, R.; Bradac, C. Effects of microstructure and growth conditions on quantum emitters in gallium nitride. *APL Mater.* **2019**, *7*, 081106.
- (5) Xue, Y.; Wang, H.; Xie, N.; Yang, Q.; Xu, F.; Shen, B.; Shi, J.-j.; Jiang, D.; Dou, X.; Yu, T.; Sun, B.-q. Single-Photon Emission from Point Defects in Aluminum Nitride Films. *J. Phys. Chem. Lett.* **2020**, *11*, 2689–2694.
- (6) Lienhard, B.; Lu, T.-J.; Jeong, K.-Y.; Moon, H.; Iranmanesh, A.; Grosso, G.; Englund, D. High-purity single photon emitter in aluminum nitride photonic integrated circuit. *2017 Conference on Lasers and Electro-Optics Europe and European Quantum Electronics Conference*, OSA, 2017; pp 1–1.
- (7) Gruber, A.; Dräbenstedt, A.; Tietz, C.; Fleury, L.; Wrachtrup, J.; von Borczyskowski, C. Scanning Confocal Optical Microscopy and Magnetic Resonance on Single Defect Centers. *Science* **1997**, *276*, 2012–2014.
- (8) Kurtsiefer, C.; Mayer, S.; Zarda, P.; Weinfurter, H. Stable Solid-State Source of Single Photons. *Phys. Rev. Lett.* **2000**, *85*, 290–293.
- (9) Naydenov, B.; Dolde, F.; Hall, L. T.; Shin, C.; Fedder, H.; Hollenberg, L. C. L.; Jelezko, F.; Wrachtrup, J. Dynamical decoupling of a single-electron spin at room temperature. *Phys. Rev. B: Condens. Matter Mater. Phys.* **2011**, *83*, 081201.
- (10) Falk, A. L.; Klimov, P. V.; Buckley, B. B.; Ivády, V.; Abrikosov, I. A.; Calusine, G.; Koehl, W. F.; Gali, Á.; Awschalom, D. D. Electrically and Mechanically Tunable Electron Spins in Silicon Carbide Color Centers. *Phys. Rev. Lett.* **2014**, *112*, 187601.
- (11) Lohrmann, A.; Iwamoto, N.; Bodrog, Z.; Castelletto, S.; Ohshima, T.; Karle, T.; Gali, A.; Prawer, S.; McCallum, J.; Johnson, B. Single-photon emitting diode in silicon carbide. *Nat. Commun.* **2015**, *6*, 7783.

- (12) Widmann, M.; et al. Coherent control of single spins in silicon carbide at room temperature. *Nat. Mater.* **2015**, *14*, 164–168.
- (13) Pernice, W. H. P.; Xiong, C.; Schuck, C.; Tang, H. X. Second harmonic generation in phase matched aluminum nitride waveguides and micro-ring resonators. *Appl. Phys. Lett.* **2012**, *100*, 223501.
- (14) Xiong, C.; Pernice, W. H. P.; Sun, X.; Schuck, C.; Fong, K. Y.; Tang, H. X. Aluminum nitride as a new material for chip-scale optomechanics and nonlinear optics. *New J. Phys.* **2012**, *14*, 095014.
- (15) Lu, T.-J.; Fanto, M.; Choi, H.; Thomas, P.; Steidle, J.; Mouradian, S.; Kong, W.; Zhu, D.; Moon, H.; Berggren, K.; Kim, J.; Soltani, M.; Preble, S.; Englund, D. Aluminum nitride integrated photonics platform for the ultraviolet to visible spectrum. *Opt. Express* **2018**, *26*, 11147.
- (16) Wan, N. H.; Lu, T.-J.; Chen, K. C.; Walsh, M. P.; Trusheim, M. E.; De Santis, L.; Bersin, E. A.; Harris, I. B.; Mouradian, S. L.; Christen, I. R. Large-scale integration of near-indistinguishable artificial atoms in hybrid photonic circuits. *arXiv preprint arXiv:1911.05265* **2019**, na.
- (17) Tu, Y.; Tang, Z.; Zhao, X. G.; Chen, Y.; Zhu, Z. Q.; Chu, J. H.; Fang, J. C. A paramagnetic neutral V Al O N center in wurtzite AlN for spin qubit application. *Appl. Phys. Lett.* **2013**, *103*, 072103.
- (18) Seo, H.; Govoni, M.; Galli, G. Design of defect spins in piezoelectric aluminum nitride for solid-state hybrid quantum technologies. *Sci. Rep.* **2016**, *6*, 20803.
- (19) Varley, J. B.; Janotti, A.; Van de Walle, C. G. Defects in AlN as candidates for solid-state qubits. *Phys. Rev. B: Condens. Matter Mater. Phys.* **2016**, *93*, 161201.
- (20) Bowes, P. C.; Wu, Y.; Baker, J. N.; Harris, J. S.; Irving, D. L. Space charge control of point defect spin states in AlN. *Appl. Phys. Lett.* **2019**, *115*, 052101.
- (21) Faraon, A.; Barclay, P. E.; Santori, C.; Fu, K.-M. C.; Beausoleil, R. G. Resonant enhancement of the zero-phonon emission from a colour centre in a diamond cavity. *Nat. Photonics* **2011**, *5*, 301–305.
- (22) Jardin, C.; Canut, B.; Ramos, S. M. M. The luminescence of sapphire subjected to the irradiation of energetic hydrogen and helium ions. *J. Phys. D: Appl. Phys.* **1996**, *29*, 2066–2070.
- (23) Davydov, V. Y.; Kitaev, Y. E.; Goncharuk, I. N.; Smirnov, A. N.; Graul, J.; Semchinova, O.; Uffmann, D.; Smirnov, M. B.; Mirgorodsky, A. P.; Evarestov, R. A. Phonon dispersion and Raman scattering in hexagonal GaN and AlN. *Phys. Rev. B: Condens. Matter Mater. Phys.* **1998**, *58*, 12899–12907.
- (24) McNeil, L. E.; Grimsditch, M.; French, R. H. Vibrational Spectroscopy of Aluminum Nitride. *J. Am. Ceram. Soc.* **1993**, *76*, 1132–1136.
- (25) Wang, H.; et al. Towards optimal single-photon sources from polarized microcavities. *Nat. Photonics* **2019**, *13*, 770–775.
- (26) Neumann, P.; Beck, J.; Steiner, M.; Rempp, F.; Fedder, H.; Hemmer, P. R.; Wrachtrup, J.; Jelezko, F. Single-Shot Readout of a Single Nuclear Spin. *Science* **2010**, *329*, 542–544.
- (27) Maze, J. R.; Stanwix, P. L.; Hodges, J. S.; Hong, S.; Taylor, J. M.; Cappellaro, P.; Jiang, L.; Dutt, M. V. G.; Togan, E.; Zibrov, A. S.; Yacoby, A.; Walsworth, R. L.; Lukin, M. D. Nanoscale magnetic sensing with an individual electronic spin in diamond. *Nature* **2008**, *455*, 644–647.
- (28) Kraus, H.; Soltamov, V. A.; Fuchs, F.; Simin, D.; Sperlich, A.; Baranov, P. G.; Astakhov, G. V.; Dyakonov, V. Magnetic field and temperature sensing with atomic-scale spin defects in silicon carbide. *Sci. Rep.* **2015**, *4*, 5303.
- (29) Plakhotnik, T.; Moerner, W.; Palm, V.; Wild, U. P. Single molecule spectroscopy: maximum emission rate and saturation intensity. *Opt. Commun.* **1995**, *114*, 83–88.